Materials Research. 2021; 24(3): e20210055
DOI: https://doi.org/10.1590/1980-5373-MR-2021-0055

Investigation on Internal Crack Defects in Medium Carbon Steel by Soft Reduction

Naqash Ali[a], *Liqiang Zhang*[a*], *Hongwei Zhou*[b], *Aonan Zhao*[a], *Chaojie Zhang*[a], *Kaixuan Fu*[a], *Jinqi Cheng*[a]

[a]*Anhui University of Technology, School of Metallurgical Engineering, Maanshan, China.*
[b]*Anhui University of Technology, School of Materials Science and Engineering, Maanshan, China.*

Received: January 20, 2021; Revised: February 08, 2021; Accepted: February 16, 2021

This paper investigated the effect of soft reduction amount increasing from 1-4mm with a cooling time of 120s and 180s to reduce the internal crack defects by analyzing the microstructure, crack morphology, extent and nature of grain boundary ferrite, centre macrosegregation, and fracture surfaces in medium carbon steel. It was found that the large extent of grain boundary ferrite with coarse morphology weakens the bonding force of the PAGB and makes it brittle with the initiation of micro-cracks. The sever centre carbon macrosegregation of 1.3 takes place at cooling time of 180s with different reduction amounts, which becomes homogeneous at cooling time of 120s. The results show that the length of inter-granular and trans-granular cracks reaches 20mm with the carbon macrosegregation index of 1.3. The carbon macrosegregation index of 1.3 with a small fraction of 15% is enough to deteriorate the centre macrostructure of the ingot. The cleavage facet size of fracture surfaces is remarkably decreased below 100um at soft reduction parameters of 2mm/120s, 3mm/120s, and 4mm/120s with micro-cracks less than 100um, which reveals that the microstructure of specimens with these soft reduction parameters is more resistant to the cracks propagation.

Keywords: *Medium carbon steel, soft reduction, internal crack defects, grain boundary ferrite, carbon macrosegregation.*

1. Introduction

With the passage of time, our requirements for high-quality steel are increasingly constant. Therefore, it's essential to discover the different ways to meet high quality steel. The internal crack defects have been long known as a major problem in the continuous casting process, and it is quite complicated to find the factors, which are responsible for their formation. The soft reduction technique has been proved to reduce central defects and segregation in continuous casting steel. The SR amount was calculated based on the compensation of solidification shrinkage, as a result the centerline and V segregation were improved significantly in high carbon bloom[1]. Macrosegregation quality criteria were simulated to study the effect of mechanical soft reduction on the slab centerline segregation. The results indicated that MSR based on casting speed can improve the quality of centerline areas in different ways[2]. The optimization measures with different soft reduction parameters are focused to improve the centre quality of steel[3-5]. Soft reduction is an effective method to eliminate the centre macrosegregation and shrinkage cavity, but improper SR parameters lead to internal cracks. During the operation of the continuous caster, external forces (including thermal and mechanical stresses) act on the fragile liquid-solid interface causes the deformation of the bloom, and cracks will occur when the deformation exceeds the allowable limit. Zong et al.[6] found two major types of cracks in dimension and inclination. The shear stress and maximum tensile stress were concentrated at the boundary of the brittle temperature region in the longitudinal and transverse section of bloom respectively, resulted in the formation and propagation of cracks. The morphology, factors affecting and formation mechanism of surface and internal cracks in continuous casting steel have been studied by several researchers[7-12]. Wang et al.[13] developed a thermo-mechanical finite element model to investigate the effect of soft reduction on internal crack formation. The results showed that internal cracks can be initiated during the solidification process when the concentrated strain exceeded the critical strain or the applied tensile stress exceeded the critical fracture stress. In this paper, the internal crack defects in medium carbon ingot were analyzed by soft reduction parameters. The results show that the microstructural features, extent and morphology of grain boundary ferrite and the carbon macrosegregation have a significant effect on the formation of internal crack defects. Therefore, the optimized SR parameters are proposed to reduce the internal crack defects in order to improve the quality of ingot.

2. Materials and Methods

Soft reduction experiments were carried out on medium carbon steel ingot to investigate the formation and control of internal crack defect by microstructure analysis, crack morphology, the extent of ferrite along prior austenite grain boundary, carbon macrosegregation, and fracture surface analysis. The schematic of soft reduction experiment and

*e-mail: zhangsir508@163.com

average composition (wt.%) of the medium carbon steel is shown in Tables 1 and 2 respectively. The physical model diagram of the experimental setup is shown in Figure 1. The scrap was put into the graphite corundum crucible and then placed in the vacuum crucible furnace (VCB-1700) at a temperature of 1600 °C to prepare the molten metal. The molten metal was taken out from the furnace and cooled in air for 120s and 180s according to the experimental scheme as shown in Table 1. The samples were quenched in water after applying the reduction amounts at room temperature (25 °C). The molten metal was only air-cooled without the implementation of reduction amount in case of reference experiment. The ingot shell will solidified earlier with a rapid decrease of temperature from 1600°C to about 900-1100°C due to the air cooling for 120s, and further decreases at high cooling time of 180s. The ingot center still has a high temperature due to the molten metal before the implementation of SR amount. Therefore, a non-uniform temperature gradient exists from surface toward the center of ingot, which mainly depend on the cooling times. The main purpose of soft reduction is to compensate the solidification shrinkage at the center of ingot by the motion of molten metal toward the core of ingot, which will be less effective at high cooling time due to the complete ingot solidification before the implementation of reduction amounts.

The width of ingots depend upon the original diameter of corundum crucible as 40mm, while the height of ingot is variable depending on the weight of scrap ranging from 400-550g as shown in Table 1. All the samples were cut into two halves from the longitudinal section of ingot, then fine ground, polished and etched with 1:1 HCL and warm water solution to reveal the macrostructure.

The small specimens of 15×15×10mm^3 were prepared from the one half of the ingot with crack region, then these specimens were fine ground, polished with diamond paste and followed by 4 vol.% nital etching for microstructure analysis and crack morphology. Field emission scanning electron microscope (FESEM NANO 430) was used for microstructure characterization, while the electron backscattering diffraction (EBSD; HKL channel 5 with an acceleration voltage of 20 kV) equipped with SEM (Zeiss Sigma 500) was used to analyze the extent and morphology of grain boundary ferrite. The other half of ingot was used to determine the centre carbon, sulphur and silicon macrosegregation of ingot with original position statistic distribution analysis (OPA-200). The specimens with a size of 30×15×10mm^3 were cut for fracture test, beneath the surface of ingot selected for OPA analysis. These specimens were dip in liquid nitrogen and broke from the centre with pliers to observe the fracture surface by scanning electron microscope (SEM).

Table 1. Schematic of ingot soft reduction experiment.

	Reduction amount (mm)	Weight of scrap before melting, (g)	Air cooling time (s)	(Width×Height) (mm)
			before SR	after SR
Case 1	1	504	120	40×50
	2	501.4	120	40×50
	3	402	120	40×40
	4	546.7	120	40×55
Case 2	1	562	180	40×57
	2	551	180	40×55
	3	602.3	180	40×60
	4	548	180	40×55
	Without SR	466	Direct WQ	40×46

Table 2. The chemical composition of medium carbon steel (wt.%).

C	Mn	Si	P	S	Cr	Ni
0.60	0.65	0.27	≤ 0.035	≤0.035	≤0.25	≤0.30

3. Results and Discussion

3.1. Structure analysis and crack morphology

Figure 2 shows the macrographs of each specimen show the internal cracks and shrinkage cavity with and without SR. The resulting cracks are inter-granular and trans-granular, which are originating from the shrinkage cavity at the centre of ingot. The internal crack and shrinkage cavity can be avoided by optimizing the reduction parameters by appropriate reduction amount to the area adjacent to liquid core. In contrast to the ingot at reduction amount of 2mm and 4mm with cooling time of 120s, the centre shrinkage cavity is eliminated and internal cracks can be reduced to a large extent, which are mainly transverse cracks growing towards the center of ingot. Transverse cracking is mainly due to intermediate temperature embrittlement.

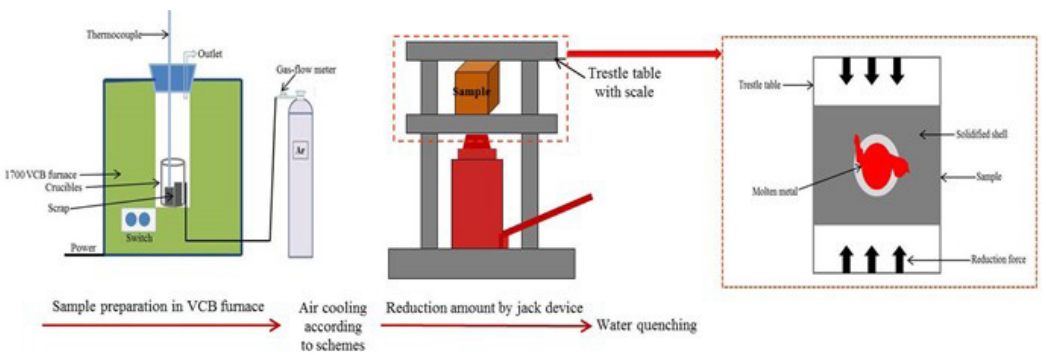

Figure 1. The physical model diagram of the experimental setup.

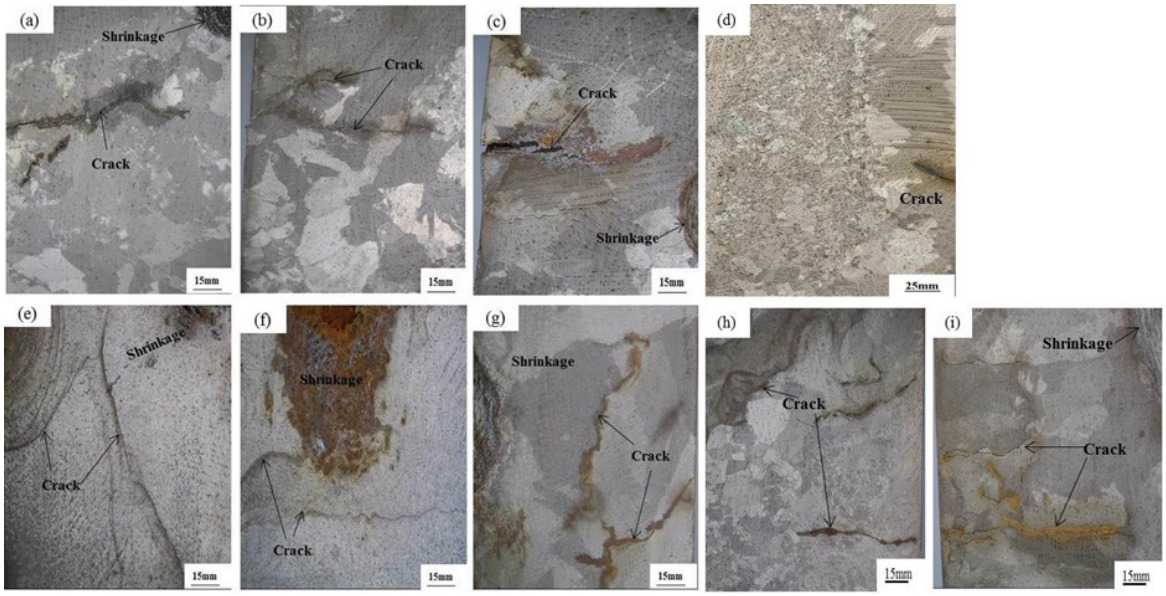

Figure 2. Micrographs of crack region at the centre of ingot, (a-d) With cooling time of 120s and SR of 1mm, 2mm, 3mm and 4mm, respectively; (e-h) With cooling time of 180s with SR of 1mm, 2mm, 3mm and 4mm, respectively and (i) Without SR.

The temperature is lowest at the corner of the ingot, which makes the corners to resist against deformation. Therefore, the effective deformation is produced in the centre of the ingot to minimize centre segregation and porosity[14].

Figure 3 shows FESEM images along the prior austenite grain boundary (PAGB), which reveals the dominant formation of grain boundary ferrite (GB-α). The pro-eutectoid ferrite is detrimental to the slab ductility due to the plastic deformation resistance formed along the former PAGB during the austenite/ferrite transition[15]. The lath martensite microstructure is due to the high-temperature heat treatment and water quenching treatment. Figure 3a shows three laths growing from the same inclusion to form a typical ‘‘Widmanstten (WF) star” and two of them are growing in opposite directions but the remaining one lath is differently oriented. The degenerated pearlite (DP) also nucleate from the other inclusion and grows up between the WF and pearlite block[16]. Figure 3b and 3c shows the nucleation of pearlite blocks at the prior austenite grain boundary separated by GB-α. Figure 3d reveals a small zigzag morphology of trans-granular crack in the vicinity of proeutectoid ferrite at 3mm/120s. The crack propagates across the martensite laths and stop advancing further when meets with the high angle boundaries of lath martensite. The film-like pro-eutectoid ferrite is precipitated in the crack, which leads to the stress concentration under the action of small thermal or deformation stress and secondary cracks will originate from the main crack. The formation of secondary cracks consumes some part of the energy, as a result the stress concentration at the tip of main crack will reduce, which controls the propagation of main crack[17].

Figure 4 shows the SEM microstructure of the inter-granular crack at 4mm/120s, which is distributed along the austenite grain boundary. The crack propagation direction changes frequently and forms a zigzag morphology with a small crack at the tip of the main crack acting as a nucleation site. The EDS spectrum reveals that the crack is filled with angular and circular Al_2O_3 inclusions and has high carbon segregation. Therefore, the carbon macrosegregation will have a direct relationship with the crack formation, which is further clarified in the next section. The angular Al_2O_3 inclusion in the crack region tends to initiate micro-cracks under the fatigue loading, which are detrimental to the mechanical properties caused by the difference of thermal expansion and hardness between the matrix and inclusions[18].

3.2. Pro-eutectic ferrite precipitation along the austenite grain boundary

In order to obtain more insight into the microstructure, the electron backscatter diffraction (EBSD) comparative results at a step size of 0.2um are provided in Figure 5 and 6 at 3mm/120s and 3mm/180s respectively, which shows the grain boundary inverse pole figure (IPF) with the distribution of low angle grain boundary (LAGB 2-15° represented by red lines) and high angle grain boundaries (HAGB >15° represented by black lines). Both cases indicate a continuous grain boundary ferrite GB-α precipitation with different morphology and extent at the low and high cooling time with the same reduction amounts.

Figure 6 shows a high extent of GB-α precipitation at 3mm/180s, which becomes less at 3mm/120s with its growth in one neighboring grain as shown in Figure 5. Furthermore, the morphology of GB-α precipitation is also different in both cases at the different cooling times. The GB-α forms at the prior austenite grain boundary (PAGB) and grows into its neighboring grains due to the different orientation relationship. At 3mm/120s, the fine GB-α grows into one adjacent prior austenite grain The GB-α moves along the PAGB in a step wise manner possessing a large fraction of HAGB, which controls its further growth along the grain boundary and inside of the grain. At 3mm/180s, the GB-α continuously grows along PAGB and its growth is also dominant in both of adjacent grains, which covers almost

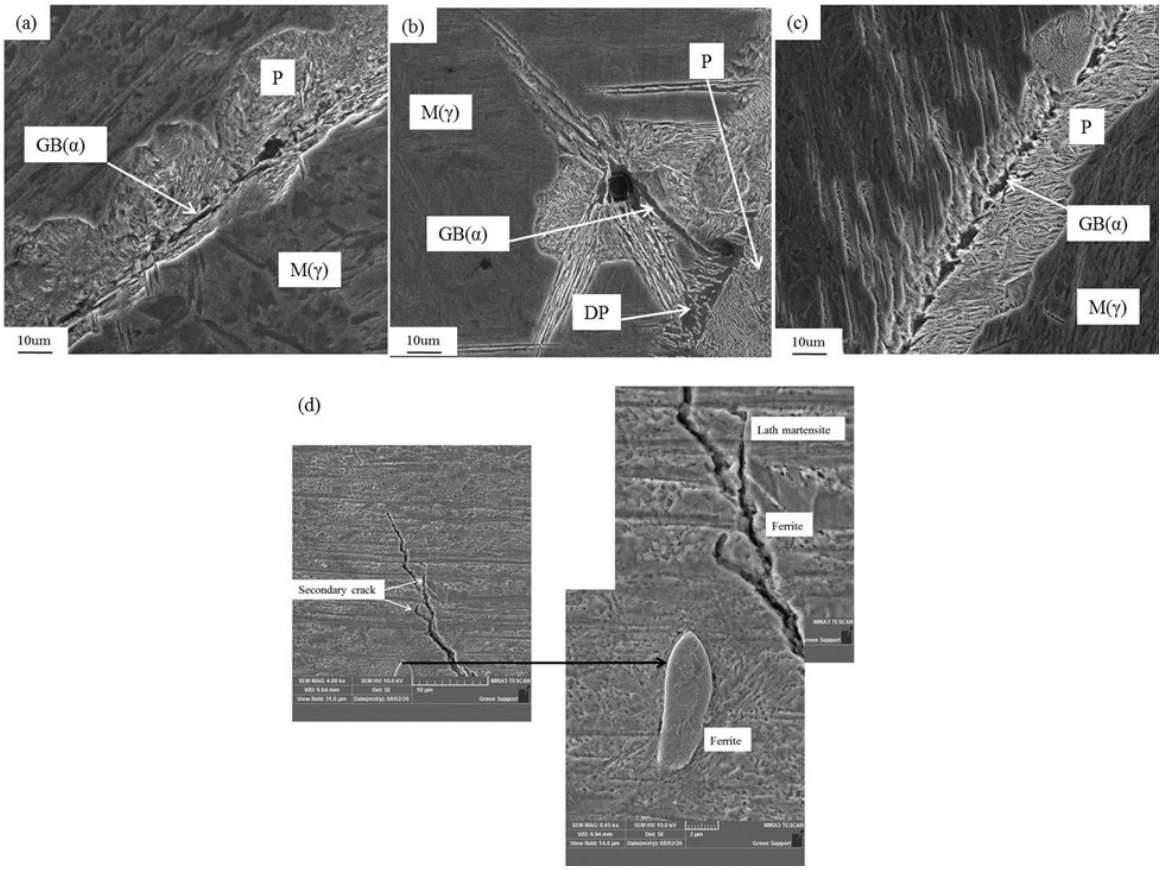

Figure 3. Microstructures of specimens, (a) At 3mm/120s, (b) At 3mm/180s, (c) Without SR and, (d) Crack morphology at 3mm/120s.

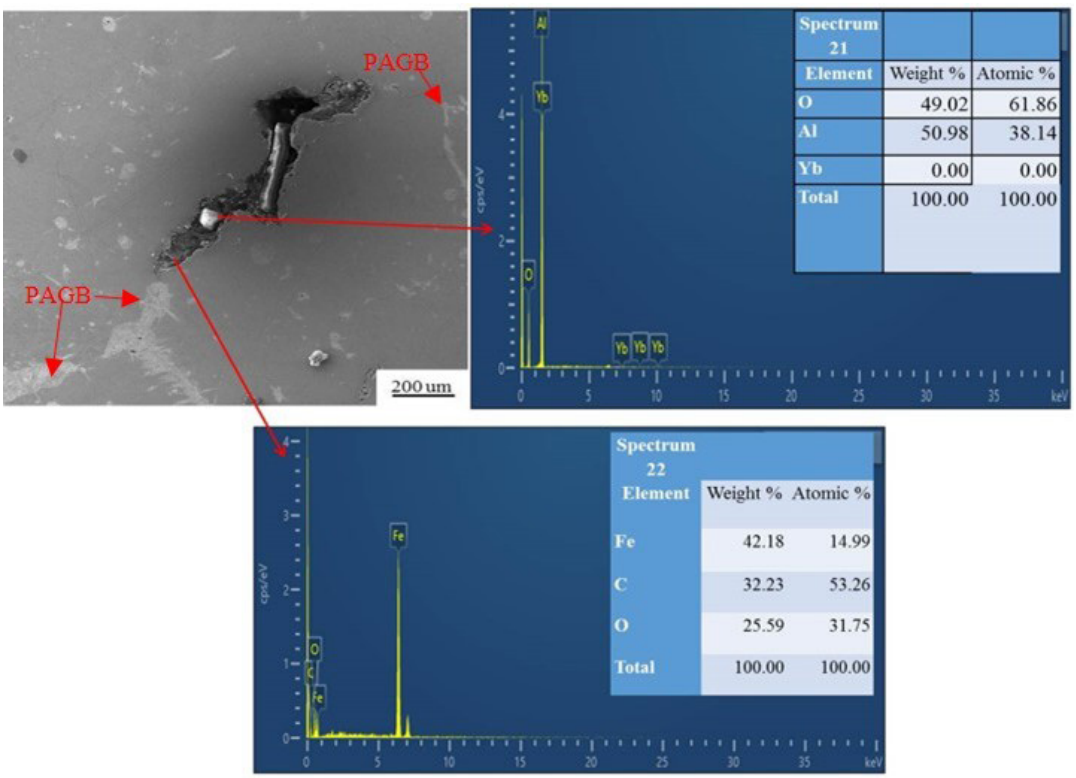

Figure 4. SEM image and EDS of the crack region at 4mm/120s.

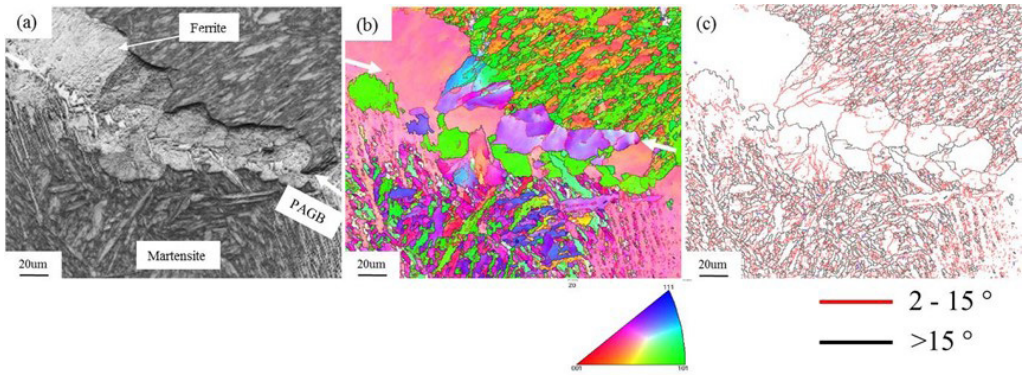

Figure 5. Grain boundary ferrite morphology at 3mm/120s, (a) SEM image, (b) inverse pole figure (IPF), (c) angle distribution.

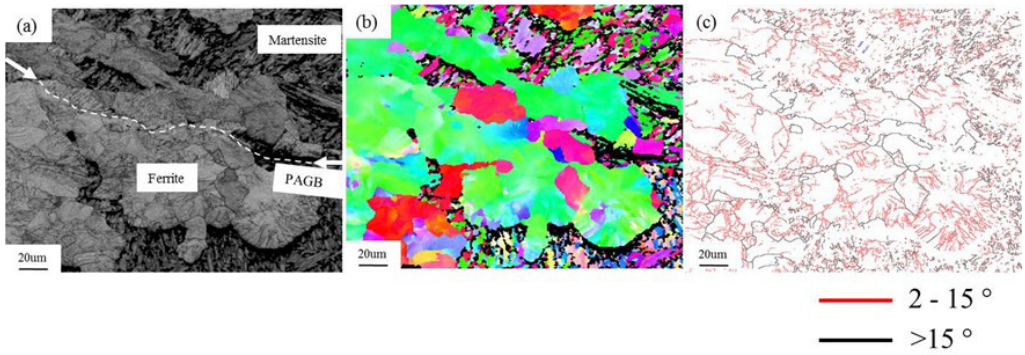

Figure 6. Grain boundary ferrite morphology at 3mm/180s, (a) SEM image, (b) inverse pole figure (IPF), (c) angle distribution.

whole lower grain. The coarse and blocky morphology of GB-α is attributed to the high fraction of LAGBs. Furthermore, there can be a same orientation relationship between WF from Figure 3b and GB-α, which indicates that the WF is necessity to decrease the boundary energy against both of the neighboring grains, as a result the formation of low angle grain boundaries. The HAGBs is also beneficial at this SR parameter as it tries to control the vigorous growth of grain boundary ferrite along PAGB and inside of the grain. In both cases, the lath martensite also possesses HAGBs, which is beneficial to control the main crack length.

Therefore, it can be inferred that the low cooling time of 120s with a high fraction of HAGBs leads to controlled growth of GB-α precipitation by lowering its continuity, as compared with the high cooling time of 180s. The strength of GB-α precipitation is much less, which leads to stress concentration at the austenite grain boundary under the action of thermal or deformation stresses. Therefore, the bonding force of the austenite grain boundary reduces and the thermo-plasticity of steel ingot rapidly deteriorates. The grain boundary becomes brittle with the initiation of micro-cracks from it.

3.3. Carbon macrosegregation

After the implementation of different reduction amounts, carbon macrosegregation is an important factor to control the internal quality of ingot. The concentration and distribution of carbon in the cross-section of the ingots could be obtained directly by original position static distribution analysis (OPA). The mechanism of central segregation by soft reduction technique is mainly due to three aspects; (1) Selective crystallization during the solidification process, (2) The flow of solute-rich molten steel toward the core of ingot, and (3) The change in the solidified structure of ingot during the solidification process. Therefore, the solubility of carbon in solid and liquid phases becomes variable, resulting in the non-uniform chemical composition with higher carbon content at the centre of ingot than the other areas. Figure 7i and 7j represents the two-dimensional contour map of carbon concentration in the cross-section of ingots with different reduction amounts and cooling time. Soft reduction amounts of 2mm and 4mm with a low cooling time of 120s, work effectively to compensate for the solidification shrinkage in the core of ingot, as a result uniform carbon distribution with less segregation was obtained as shown in Figure 7b and d. The higher diffusion of carbon content to the ingot center is responsible for the formation of widsmanstatten ferrite (WF) plates, originating from the austenite grain boundaries as shown in Figure 3a. The WF plates are produced at very high temperatures and are attributed to the higher carbon diffusivity at these temperatures[19]. The aggregates of parallel growing WF plates nucleate from the austenite grain boundary with identical orientation and the cleavage crack can easily pass from the cluster of these plates to deteriorate the microstructure[20]. Therefore, the higher cooling time before implementation of SR amount increases the carbon macrosegregation with the formation of shrinkage cavity (with a high fraction of red area in OPA pictures) at the core of ingot as shown in Figure 7e-i. The center segregation and shrinkage cavity are closely related to the thickness of the solidified shell,

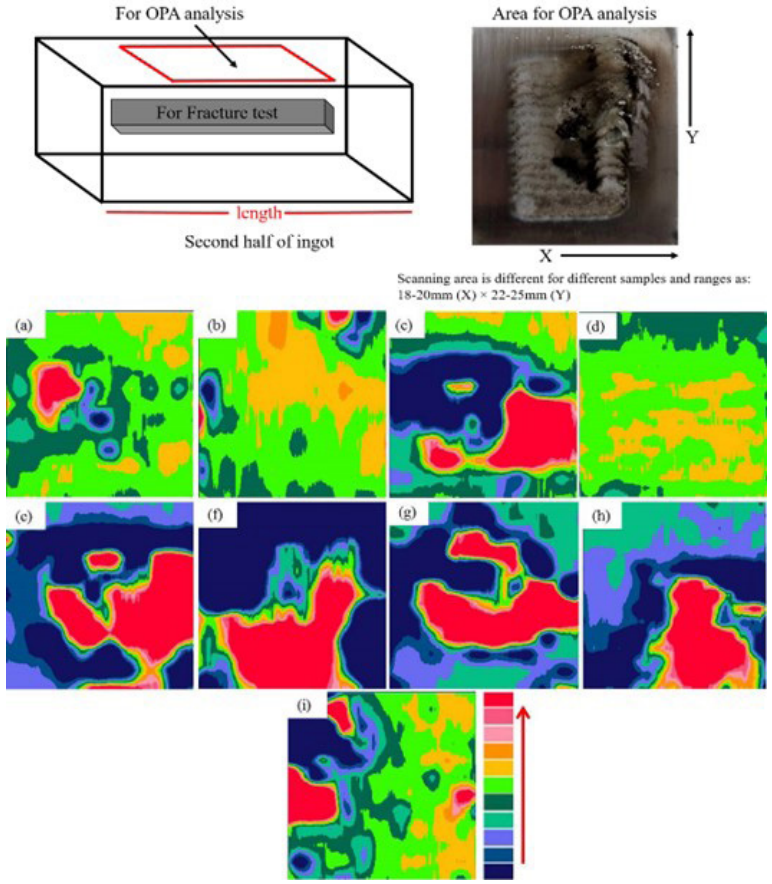

Figure 7. Two-dimensional contour map of carbon macrosegregation in the longitudinal section of ingot, (a-d) 120s with SR of 1mm, 2mm, 3mm and 4mm, respectively; (e-h) 180s with SR of 1mm, 2mm, 3mm and 4mm, respectively and (i) Without SR.

which reveals the incomplete solidification process with a higher temperature at the ingot centre than the edge regions.

The eccentricity of the carbon content in the experimental steel is more serious, which significantly drops the endpoint temperature, as a result the solid phase at the ingot centre also reduces. Therefore, the reduction amount at higher cooling time of 180s was not enough to compensate for the solidification shrinkage, as the applied reduction amounts produce a negative pressure, which causes the motion of liquid steel enriched with carbon content toward the core of ingot, resulting in the formation of shrinkage cavity and non-uniform carbon segregation. The centre segregation is due to compensation of volume change in the centre of ingot by the liquid steel which comes partially from interdendritic areas during the formation of shrinkage cavity[21]. Figure 8 illustrates the fractions of carbon macrosegregation indexes in the middle of ingot with different soft reduction parameters. The fractions of carbon macrosegregation index are 24%, 17%, and 20% with macrosegregation index of 1.3 at reduction amount of 1mm, 2mm, and 4mm respectively, with cooling time of 180s. This implies that the transportation of interdendritic liquid metal to the centre of ingot with larger cooling time increases the final centre macrosegregation and crack defects during the formation of shrinkage cavity. Without SR, the macrosegregation index exceeds above 1.3 containing volume fraction of 15% as shown in Figure 8b. The fraction of carbon macrosegregation indexes does not exceed above 1.2 at reduction amounts of 1-4mm with low cooling time of 120s as shown in Figure 8a. The carbon content is homogeneously distributed in sample #2 and #4 with a macrosegregation index less than 1.12 across the whole scanned area. Figure 9 illustrates the length of the cracks at different carbon macrosegregation indexes. The length of internal cracks increases up to 20mm when the carbon macrosegregation index reaches to 1.3. Figure 10 indicates the maximum segregation degree of S and Si at different reduction amounts and cooling time, which also have a significant effect on the macrostructure of investigated steel.

From the above analysis, it can be inferred that the carbon macrosegregation index exceeding above 1.2 is dertrimantal to the microstructure, as the inter and trans-granular cracks at the centre of ingot start to initiate from the shrinkage cavity and their growth increases when the carbon macrosegregation index reaches to 1.3. Also, the macrosegregation index of 1.3 with a small fraction above 15% is enough to deteriorate the centre macrostructure of the ingot. Therefore, the control of carbon, sulphur, and silicon maximum macrosegregation degrees below 1.2 is an effective measure to eliminate the internal crack defects. The previous reports established a direct relationship between crack length and the centre carbon macrosegregation[10,21,22].

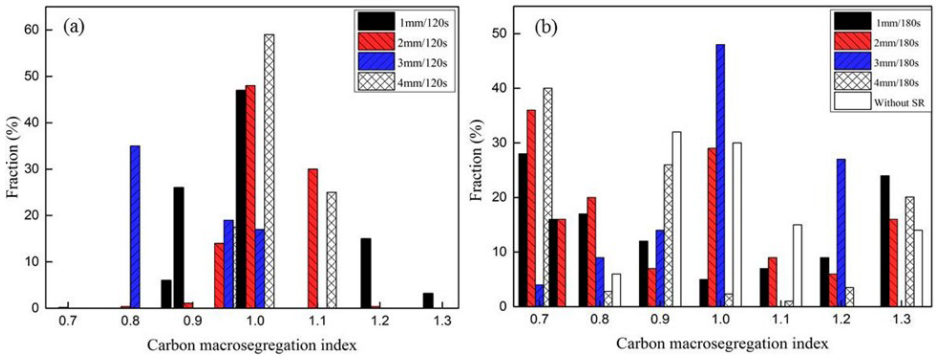

Figure 8. The fraction of different carbon macrosegregation indexes in the middle of the ingot (a) at 120s, (b) at 180s.

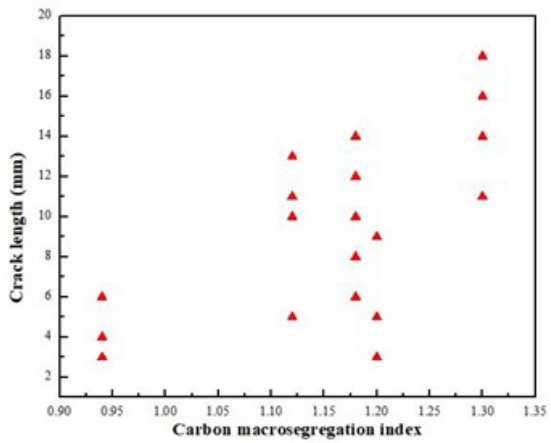

Figure 9. The relationship between carbon macrosegregation indexes and crack lengths.

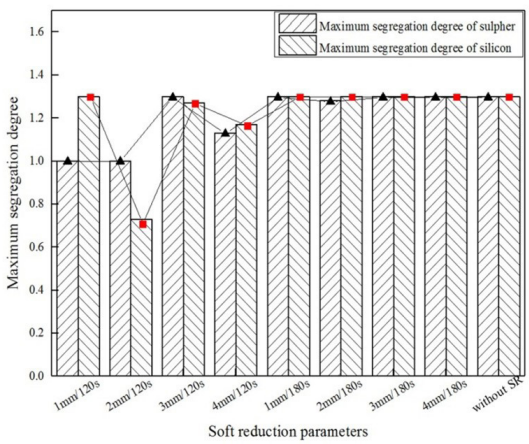

Figure 10. Maximum segregation degree of sulphur and silicon at different soft reduction parameters.

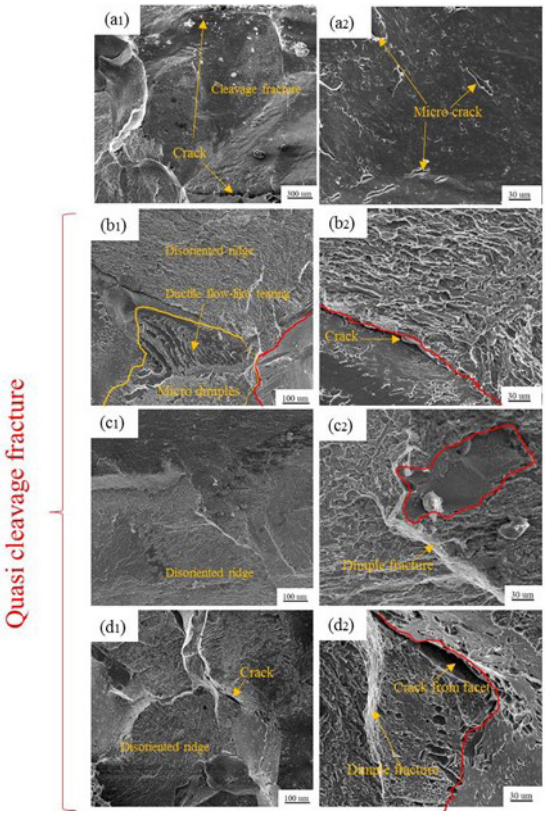

Figure 11. SEM fractographs, (a1, a2) 1mm/120s, (b1, b2) 2mm/120s, (c1, c2) 3mm/120s and (d1, d2) 4mm/120s.

3.4. Fracture surface analysis

Figures 11 and 12 illustrate the fracture surface micrographs of specimens at the cooling time of 120s and 180s respectively with different reduction amounts. The comparative fracture morphologies reveal the quasi- cleavage and brittle fracture with dominated inter-granular fracture mode. A river like pattern containing a large number of tongue-like shapes in a facet is clear in the samples at 1mm/180s and without SR technique, which reveals a high rate of imposed deformations. The different cleavage steps propagating on parallel cleavage planes merge to form a river like pattern[23].

The inter-granular fracture denoted by red lines is dominated in the crack initiation region, which weakens the grain boundary and easily initiates the cracks by acting as a path for the micro-crack propagation. The micro-cracks in all specimens may be due to the uncontrolled austenite-martensite transformation, which propagated through the austenite grains without significant changes in their propagation[24]. The inter-granular fracture area is used as a large cleavage facet

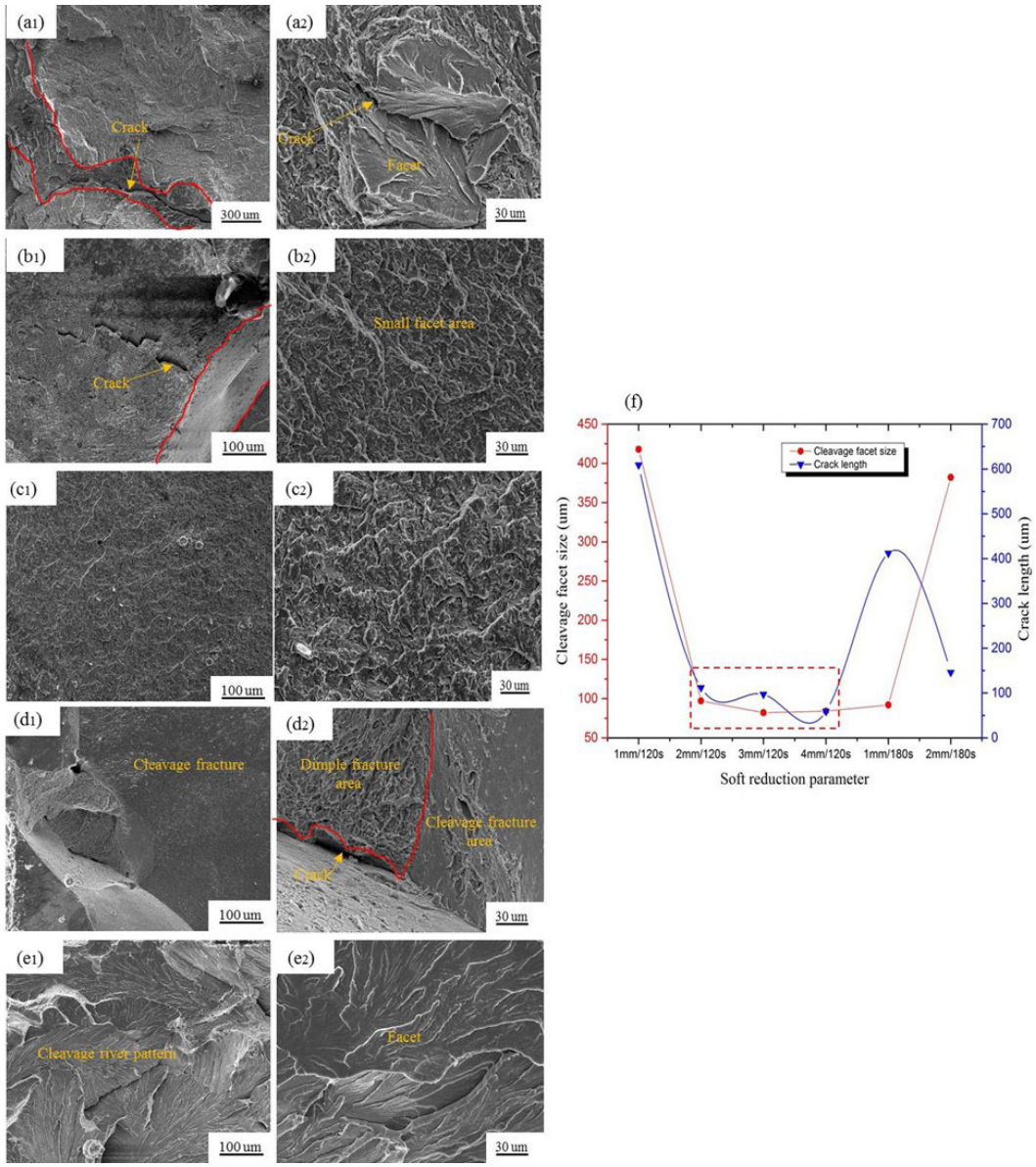

Figure 12. SEM fractographs, (a1, a2) 1mm/180s, (b1, b2) 2mm/180s, (c1, c2) 3mm/180s, (d1, d2) 4mm/180s and, (f) The relationship between cleavage facet size and crack length at cooling time of 120s and 180s with different reduction amounts.

and its average size in the fracture micrographs is measured by linear intercept method. In both cases, the crack initiates from a cleavage facet and propagates along it, and its length mainly depends upon the facet size as shown in Figure 12f. The facet size is remarkably decreased below 100um at soft reduction parameters of 2mm/120s, 3mm/120s, and 4mm/120s with micro-cracks less than 100um, which reveals that the microstructure of specimens with these parameters is more resistant to the cracks propagation. Furthermore, the ductile tears and dis-oriented ridge can be seen in Figure 11b1-d2 with a ductile flow like tearing at 2mm/120s, and the shallow dimples become deep as the reduction amount increases from 2mm to 4mm.

The specimen with reduction parameter of 1mm/120s shows a large cleavage facet area and tends to fall in case 2 with high cooling time of 180s, which are mainly brittle fracture surfaces and have a large cleavage fracture area as shown in Figure 12. The large cleavage area implies that the ingots undergo a severe deformation of the solid-liquid interface. The brittle feature in fully pearlitic steel increases with the increase of cooling time[25], while the same trend is clear in investigated medium carbon dual-phase (M+F) steel. The intergranular fracture area reflects the strength of grain boundary and the energy consumption of crack initiation[18]. Therefore it can be inferred that at the strength of austenite grain boundary along with the energy consumption of crack initiation zone should increase for soft reduction parameters of 2mm/120s, 3mm/120s and 4mm/120s, while reduce dramatically for 1mm/120s and with high cooling time of 180s at different reduction amounts. This can be attributed to

the homogeneous alloying segregation at the centre of ingot and a minimum extent of grain boundary ferrite precipitation at these soft reduction parameters.

4. Conclusions

1. The internal cracks are originated from the shrinkage cavity and show the inter-granular and trans-granular growth, which are filled with the oxide inclusions and enriched with carbon content. The small transverse cracks less than 15mm are obvious without the formation of shrinkage cavity and grow towards the centre of ingot.
2. The pro-eutectoid ferrite is precipitated along the prior austenite grain boundary with different extent and morphology. The coarse and blocky morphology of GB-α is attributed to the high fraction of LAGBs at a cooling time of 180s, which turns into fine morphology with high fraction of HAGBs at 120s. Therefore, a large fraction of HAGBs is beneficial to control the growth of GB-α along the PAGB and inside of the grain. Furthermore, the high extent of GB-α weakens the bonding force of the PAGB and the thermo-plasticity of the investigated ingot rapidly deteriorates. Therefore, the grain boundary becomes brittle with the initiation of micro-cracks from it.
3. The centre carbon macrosegregation is solely responsible for the formation of internal crack defects. the carbon macrosegregation index exceeding above 1.2 is detrimental to the microstructure, as the length of inter-granular and trans-granular cracks become larger when the carbon macrosegregation index reaches 1.3. Also, the macrosegregation index of 1.3 with its small fraction above 15% is enough to deteriorate the centre macrostructure of the ingot. Therefore, control of macrosegregation below 1.3 is necessary to reduce the internal crack defects.
4. The comparative fracture surface analysis shows quasi-cleavage fracture and brittle fracture modes at the cooling time of 120s and 180s respectively. The cleavage facet size is remarkably decreased below 100um at soft reduction parameters of 2mm/120s, 3mm/120s and 4mm/120s with micro cracks less than 100um, which reveals that the microstructure of specimens with these parameters is more resistant to the cracks propagation. This can be attributed to the homogeneous and low carbon macrosegregation at the centre of ingot with a minimized extent of grain boundary ferrite precipitation.

5. Acknowledgements

The successful completion of this project is benefited from the financial support provided by National Natural Science Foundation of China (U51874001, U1760108).

6. References

1. Ji C, Luo S, Zhu M. Analysis and application of soft reduction amount for bloom continuous casting process. ISIJ Int. 2014;54(3):504-10.
2. El-Bealy MO. Macrosegregation quality criteria and mechanical soft reduction for central quality problems in continuous casting of steel. Mater Sci Appl. 2014;5(7):724-44.
3. Wu M, Domitner J, Ludwig A. Using a two-phase columnar solidification model to study the principle of mechanical soft reduction in slab casting. Metall Mater Trans, A Phys Metall Mater Sci. 2012;43(3):945-64.
4. Rogberg B, Ek L. Influence of soft reduction on the fluid flow, porosity and center segregation in CC high carbon- and stainless steel blooms. ISIJ Int. 2018;58(3):478-87.
5. Li G, Yu W, Cai Q. Investigation of reduction pretreatment process for continuous casting. J Mater Process Technol. 2016;227:41-8.
6. Zong N, Zhang H, Liu Y, Lu Z. Analysis on morphology and stress concentration in continuous casting bloom to learn the formation and propagation of internal cracks induced by soft reduction technology. Ironmak Steelmak. 2019;46(9):872-85.
7. Sun H, Li L, Wang J, Cheng X, Zhou F. Coordinating optimisation of F-EMS and soft reduction during bloom continuous casting process for special steel. Ironmak Steelmak. 2018;45(8):708.
8. Zeng J, Chen W, Wang Q, Wang G. Improving inner quality in continuous casting rectangular billets: comparison between mechanical soft reduction and final electromagnetic stirring. Trans Indian Inst Met. 2016;69(8):1623-32.
9. Li X, Ding H, Tang Z, He J. Formation of internal cracks during soft reduction in rectangular bloom continuous casting. Int J Miner Metall Mater. 2012;19(1):21-9.
10. Zeng J, Chen WQ, Zheng HG. Analysis and control of central cracks in the bloom continuous casting of microalloy 49MnVS3 steel. Ironmak Steelmak. 2017;44(9):676-84.
11. Thome R, Harste K. Principles of billet soft-reduction and consequences for continuous casting. ISIJ Int. 2006;4(12):1839-44.
12. Moon CH, Oh KS, Lee JD, Lee SJ, Lee Y. Effect of the roll surface profile on centerline segregation in soft reduction process. ISIJ Int. 2012;52(7):1266-72.
13. Wang W, Ning L, Bülte R, Bleck W. Formation of internal cracks in steel billets during soft reduction. J UNIV SCI TECHNOL B. 2008;(15):114-119.
14. Zong N, Zhang H, Liu Y, Lu Z. Analysis of the off-corner subsurface cracks of continuous casting blooms under the influence of soft reduction and controllable approaches by a chamfer technology. Metall Res Technol. 2019;116(3):1-13.
15. Wu M, Yu H. Research of 50Mn2V continuous casting slab transverse cracking during its retarded cooling process. Eng Fail Anal. 2013;30:61-73.
16. Cheng L, Wu KM, Wan XL, Wei R. In-situ observation on the growth of Widmanstätten sideplates in an Fe – C – Mn steel. Mater Charact. 2014;1:86-94.
17. Li Q, Huang X, Huang W. EBSD analysis of relationship between microstructural features and toughness of a medium-carbon quenching and partitioning bainitic steel. J Mater Eng Perform. 2017;26(12):6149-57.
18. Yang C, Luan Y, Li D, Li Y. Effects of rare earth elements on inclusions and impact toughness of high-carbon chromium bearing steel. J Mater Sci Technol. 2019;35(7):1298-308.
19. Grewal R, Aranas C Jr, Chadha K, Shahriari D, Jahazi M, Jonas JJ. Formation of Widmanstätten ferrite at very high temperatures in the austenite phase field. Acta Mater. 2016;109:23-31.
20. Bhadeshia HKDH. Phase transformations contributing to the properties of modern steels. Bull Pol Acad Sci Tech Sci. 2010;58(2):255-65.
21. Wang W, Hu X, Ning L, Bülte R, Bleck W. Improvement of center segregation in high-carbon steel billets using soft reduction. J Univ Sci Technol B. 2006;13(6):490-6.
22. El-Bealy MO. On the formation of macrosegregation and interdendritic cracks during dendritic solidification of continuous casting of steel. Metall Mater Trans, B, Process Metall Mater Proc Sci. 2014;45(2):988-1017.
23. Mishra K, Singh A. Effect of interlamellar spacing on fracture toughness of nano-structured pearlite. Mater Sci Eng A. 2017;706(9):22-6.
24. Królicka A, Radwański K, Ambroziak A, Żak A. Analysis of grain growth and morphology of bainite in medium-carbon spring steel. Mater Sci Eng A. 2019;768(10):138446.
25. Toribio J, González B, Matos JC, Ayaso F-J. Influence of microstructure on strength and ductility in fully pearlitic steels. Metals. 2016;6(12):318-30.